CHARACTERIZATION AND CIRCUIT MODELING OF PULSE CURRENT GENERATORS FOR HEMP TESTING

X. Liu [(1)], F. Grassi [(1)], G. Spadacini [(1)], S. A. Pignari [(1)], F. Trotti [(2)], W. Hirschi [(2)]

[(1)] Department of Electronics, Information and Bioengineering, Politecnico di Milano, 20133 Milan, Italy, Email:{xiaokang.liu; flavia.grassi; giordano.spadacini; sergio.pignari}@polimi.it

[(2)] Montena Technology sa, 1728 Rossens, Switzerland, Email: {francois.trotti; werner.hirschi}@montena.com

ABSTRACT

The Pulse Current Injection (PCI) technique is foreseen by several international Electromagnetic Compatibility (EMC) standards to test the vulnerability of electrical/electronic units to intense transient electromagnetic disturbances. In this work, equivalent circuit modeling of a commercial PCI generator is addressed by using a non-intrusive characterization procedure at the external port, which does not require information on internal parameters. To this end, the PCI generator is firstly characterized in the frequency domain by using a vector network analyzer. Then a multi-goal optimization procedure is exploited to assign proper values to the involved circuit parameters. The initial voltage across the internal capacitor, which determines the pulse intensity, is then optimized for each pulse level starting from time-domain measurement under different conditions. Eventually, the proposed model is used to predict the time-domain behavior of a simplified PCI setup with *ad-hoc* injection coupler, and the simulation results show satisfactory agreement with measurements.

1. INTRODUCTION

The Bulk Current Injection (BCI) technique, which foresees to inject continuous-wave (usually modulated) RF noise currents into signal and power cables, is specified by several EMC International Standards for testing the conducted susceptibility (CS) of airborne and space equipment [1], [2] up to hundreds of megahertz. Several authors investigated the possibility to resort to this technique also to replace and/or supplement traditional radiated susceptibility (RS) procedures up to a few of gigahertz [3]-[6]. The idea is to inject RF current into the interconnecting cables to reproduce, deterministically or statistically, the noise induced at the input of the equipment under test (EUT) during a traditional radiated susceptibility test [7], [8]. Hence, these alternative procedures are efficient as long as the main coupling path leading the external noise to the input of sensitive electronic devices (which are enclosed in metallic boxes) is through interconnecting cables. This condition is satisfied up to a few of gigahertz in typical space installations, as long as components/units possibly susceptible to external interference are enclosed into metallic boxes.

Similar (BCI-like) test benches are also used to test the vulnerability of electrical/electronic units to intense transient electromagnetic disturbances, such as those due to high-altitude electromagnetic pulses (HEMP). EMC of electrical equipment threatened by HEMP disturbance has been gaining increasing attention with the rapid development of power systems. Indeed, several standards, e.g., [9], [10], include a dedicated CS test procedure foreseeing the injection at the input pins of the EUT of high-power fast transients over a wideband spectrum with specified characteristics in terms of amplitude, pulse duration, as well as rise time, with the aim to include the effects of non-linear systems. This procedure, known as Pulse Current Injection (PCI), makes use of toroidal probes to directly couple intense transient disturbances into the interconnecting cables. Although these probes are quite similar to those exploited for BCI, their design is optimized based on the characteristics of the noise to be injected. Indeed, PCI probes make use of a combination of several magnetic cores to inject an intense impulsive stress waveform characterized by large amplitude and fast transient. On the contrary, the BCI technique foresees the injection of continuous CW-modulated sinusoidal waveforms, sweeping the frequency range of interest at discrete frequency points. The two tests require significantly different injection sources in terms of time-domain behavior and frequency spectra.

In the past decade, several attempts, e.g., [11], [12], have been made to design and develop suitable devices to run the PCI test, including the pulse generator and the required injection probes. Their equivalent circuit models have also been developed starting from the actual design parameters of *ad-hoc* setup, and are verified by comparison versus real measurements. However, detailed design parameters are not always available, especially when off-the-shelf commercial generators are adopted.

This work presents the results obtained in the framework of a joint research activity between Montena Technology (Switzerland) and the EMC Group at Politecnico di Milano (Italy). The final objective of the

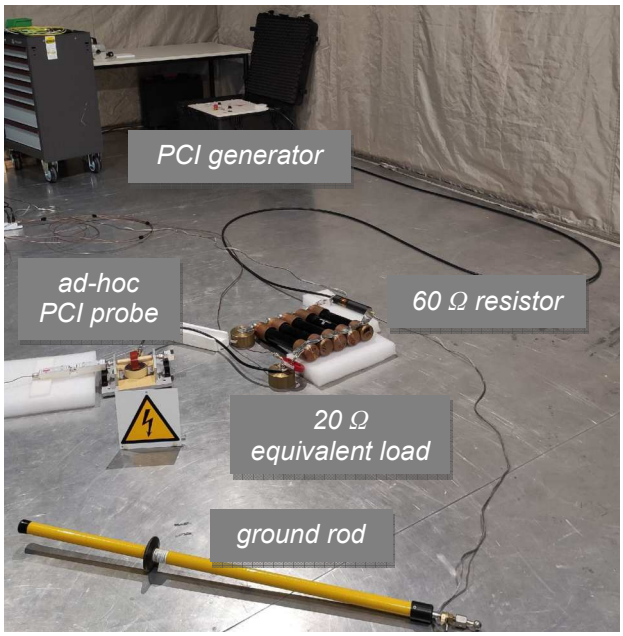

Figure 1. Picture of the PCI setup encompassing a PCI generator, load resistors, and a toroidal magnetic core mounted on the calibration jig.

research is to develop novel modelling strategies that guide the design of injection devices with enhanced characteristics in terms of maximum amplitude of the (peak) current that can be injected into the DUT. In this framework, a pre-requisite is to properly characterize the pulse current generator, so to obtain an accurate circuit representation of this device to be used for further investigation, e.g., by means of system-level co-simulation. Without loss of generality, a prototype of commercial pulse generator [13] conforming to MIL-STD-188-125 standard (see Fig. 1) is considered. Unlike previous works, where detailed information on the internal parameters were available, in this work the lack of information about the generator internal parameters is overcome by combining the results of frequency-domain measurements carried out at the generator output ports with circuit parameter optimization.

The circuit model of the pulse generator obtained in this work can be flexibly implemented in different simulation tools and used for system-level simulation of HEMP test setups according to the standards. As an illustrative example, it can be used in combination with the circuit model of a prototype PCI probe (see Fig. 1), and used to optimize its design.

2. FREQUENCY-DOMAIN CHARACTERIZATION AND CIRCUIT PARAMETER OPTIMIZATION

To determine the parameters involved in the model of the PCI generator, the internal impedance of the

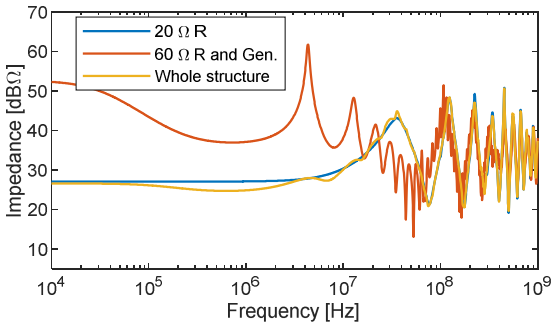

Figure 2. Measured input impedance of the PCI generator under different loading conditions.

generator is measured by a vector network analyzer with the following connected external circuits (see Fig. 2):

(1) a series 60 Ω resistor as specified by the standard to produce normalized pulse waveforms with rise time less than 20 ns and duration from 500 ns up to 550 ns;

(2) an equivalent load obtained by connecting the previous 60 Ω resistor with an additional 20 Ω resistor with high power rating. Such an additional resistor (realized by connecting five 100 Ω resistors in parallel) was included to provide a different loading condition for modeling purposes, and was preliminarily characterized by measurements.

In both cases, the input impedance can be obtained by the measured S-parameters as

$$\hat{Z}_{in}(f) = 50\frac{1+\hat{S}(f)}{1-\hat{S}(f)}\ [\Omega] \qquad (1)$$

where $\hat{S}$ is the *reflection coefficient* (complex number) at the generator input, and f denotes the frequency.

For simplicity, the 20 Ω resistor (although realized by connecting five 100 Ω resistors) is modeled by a single resistor with parasitic parameters, as shown in Fig. 3(a). According to the analysis in [11] and [12], the pulse generator is modeled by an equivalent RLC circuit [see Fig. 3(b) and (c)]. Besides, also the aluminum tapes connecting the parallel resistors and the cable connecting the resistor and the VNA are included into the circuit model, as they introduce effects no longer negligible at high frequency.

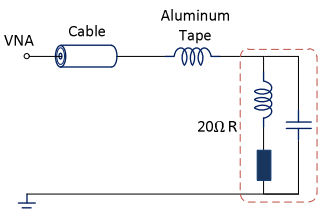

(a)

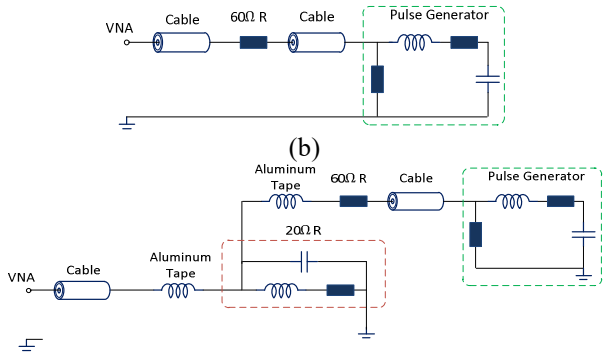

Figure 3. Circuit models of the VNA measurement setup connected to (a) the 20 Ω equivalent impedance, (b) the PCI generator with a 60 Ω resistor, and (c) the PCI generator, the 60 Ω and 20 Ω resistors.

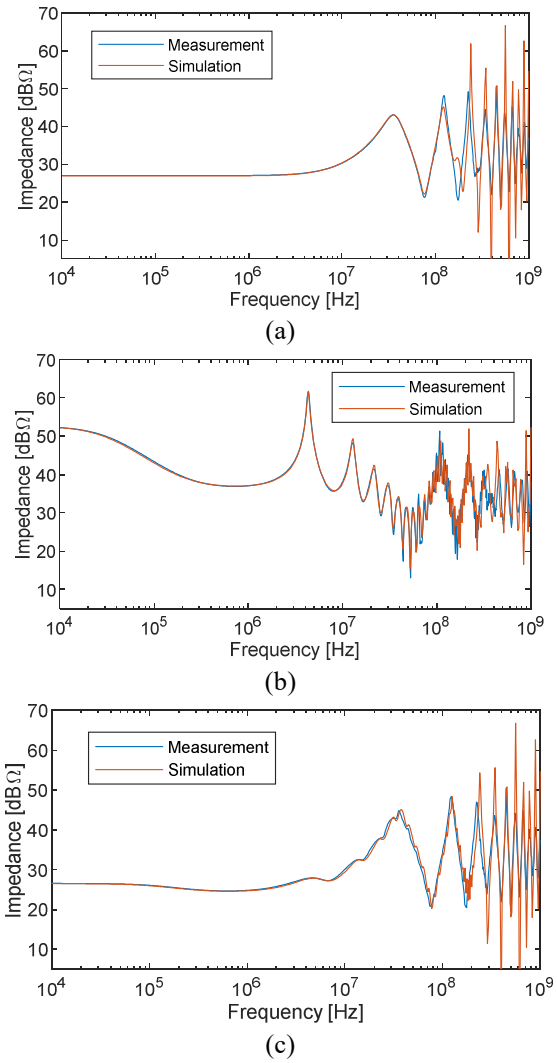

Figure 4. Prediction of the input impedance of the VNA setup when connected to (a) the 20 Ω equivalent impedance only, (b) the PCI generator with a 60 Ω resistor, and (c) the PCI generator, the 60 Ω and 20 Ω resistors.

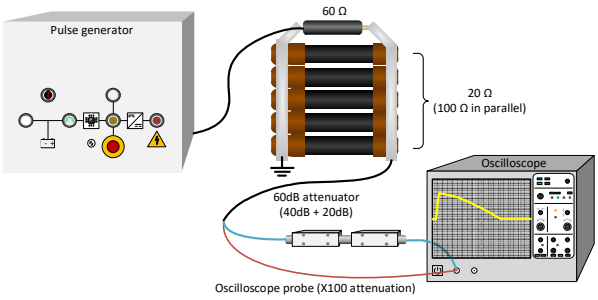

Figure 5. Schematic view of the setup for time-domain characterization of the PCI generator.

The involved circuit parameters are then optimized in ADS [14] using the embedded Genetic Algorithm. To this end, the circuit models are first built in the solver according to Fig. 3, and multiple optimization goals are set based on the measured internal impedance in Fig. 2. The target of the optimization is to achieve a good matching between simulation and measurement at discrete frequency points (100 points per decade in the interval from 10 kHz to 1 GHz). To guarantee wideband agreement, it was enforced that the following ratios,

$$R_{\mathrm{Re}}(f) = \mathrm{Re}\left[\hat{Z}_{in}^{sim}(f)\right] \Big/ \mathrm{Re}\left[\hat{Z}_{in}^{meas}(f)\right] \qquad (2)$$

$$R_{\mathrm{Im}}(f) = \mathrm{Im}\left[\hat{Z}_{in}^{sim}(f)\right] \Big/ \mathrm{Im}\left[\hat{Z}_{in}^{meas}(f)\right] \qquad (3)$$

involving the real, Re[·], and imaginary part, Im[·], of the internal impedance $Z_{in}(f)$ obtained from measurement (*meas*) and simulation (*sim*), take unitary value in the whole frequency range of interest. Hence, two goals, i.e., one for the real and one for the imaginary part, were set in the frequency interval from 10 kHz to 1 GHz.

The predicted impedances obtained by exploiting the values estimated by the optimization procedure are compared with the measured quantities (Fig. 2) in Fig. 4, showing a satisfactory agreement.

3. TIME DOMAIN CHARACTERIZATION AND INITIAL VOLTAGE OPTIMIZATION

The circuit model in Fig. 3 allows simulating different voltage levels by properly setting the initial voltage of the capacitor. To determine a proper value for such an initial voltage, time-domain measurements are carried out with two different conditions, that is with the generator connected to a 50 Ω load and left open-ended, as shown in Fig. 5.

Based on the measured voltages (see Fig. 6), the initial capacitor voltage can be optimized in MATLAB using the Pattern Search algorithm. Specifically, circuit models for the two loading conditions have been built and simulated in time domain with MATLAB/Simulink.

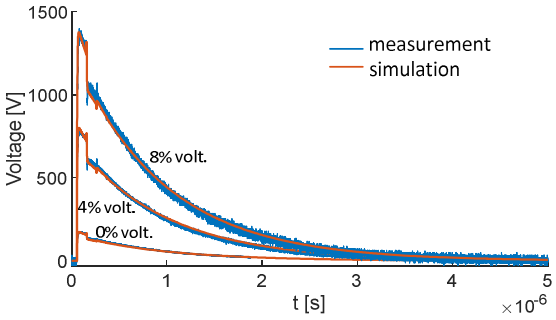

(a)

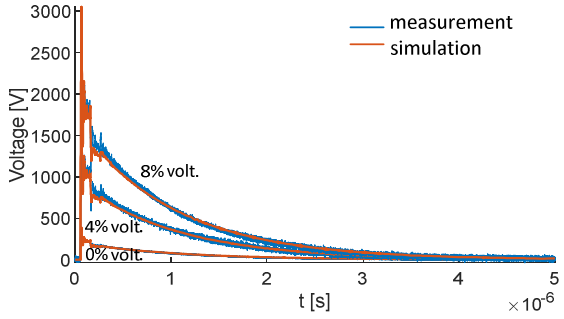

(b)

Figure 6. Time-domain voltage waveforms for different voltage levels, with the generator connected to (a) a 50 Ω load, and (b) left open-ended.

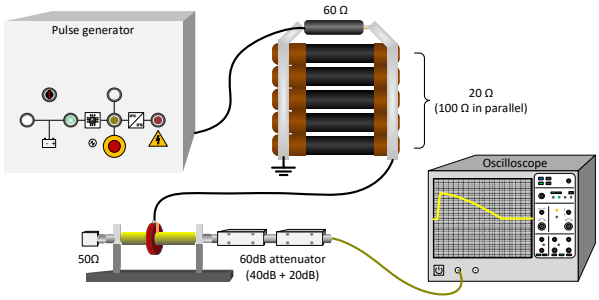

Figure 7. Principle drawing of the ad-hoc pulse-current injection measurement setup.

For each case, the integral absolute error (IAE) is calculated with a specific setting of capacitor voltage, by integrating the absolute error between the simulated and measured terminal voltages over time. The two IAE values are summed up to obtain the total error, which is the quantity to be minimized. The optimal capacitor voltage is then obtained for every PCI generator voltage setting under analysis. Examples of results are shown in Fig. 6, which put in evidence the good agreement between predictions and measurements.

4. APPLICATION EXAMPLE

As an illustrative example of application, the model of the PCI generator previously presented is here used to predict the voltage induced across a 50 Ω load in a simplified setup mimicking a pulsed current injection test bench (see Figs. 1 and 7). To this end, a hand-made inductive coupler is manufactured by winding a thin copper tape, equipped with an SMA connector, around a nanocrystalline magnetic core. Such a probe was experimentally characterized, and modeled in [15], where equivalent ladder networks were derived to represent its frequency response in the linear region. The probe is mounted onto the center conductor of a commercial calibration jig [16], whose ports are connected to a 50 Ω termination on one side, and to the oscilloscope channel on the other side.

To predict the voltage induced at the monitored termination of the jig, a Simulink-based model was exploited which combines the proposed model of the PCI generator with the probe and jig models in [15] and [16], respectively. Predictions and measurements of the induced voltage are compared in Fig. 8, where the excitation voltage ranges from the minimum voltage level allowed by the generator (labelled as '0% volt.') up to 4% of the maximum voltage the generator can generate.

These results prove the accuracy of the proposed modeling technique. It is worth noticing that the proposed validation was performed only up to 4% of the maximum voltage allowed by the generator to avoid saturation of the probe magnetic core, which is not accounted for by the exploited probe model.

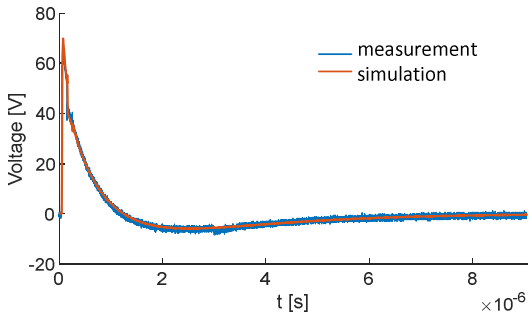

(a)

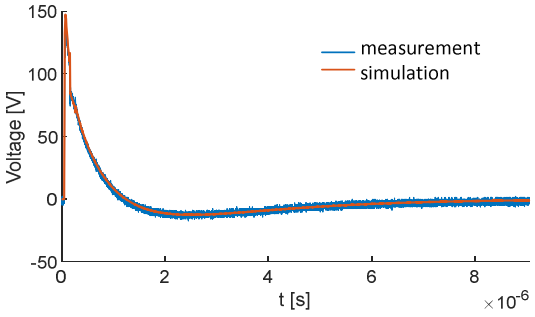

(b)

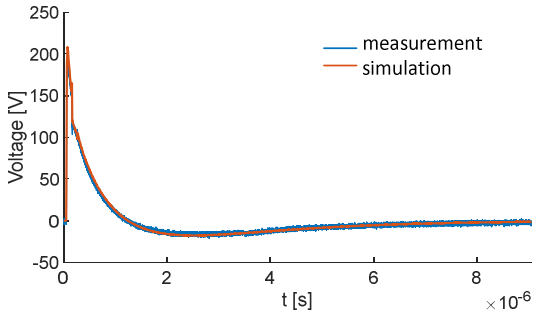

(c)

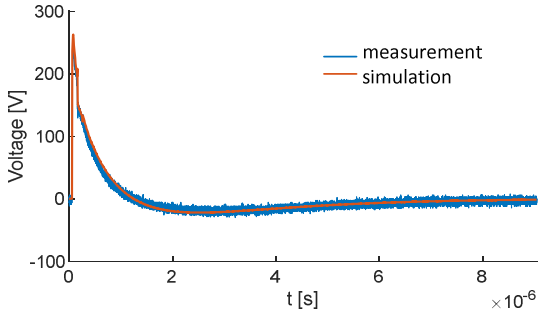

(d)

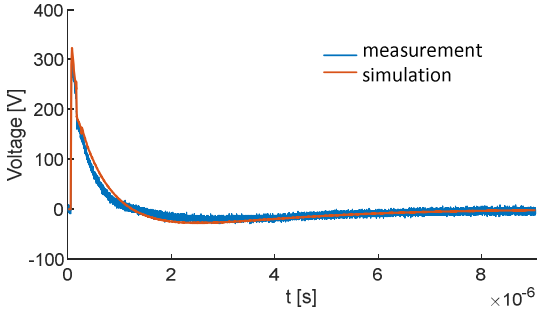

(e)

Figure 8. Voltage waveforms measured and predicted in the PCI test setup for different generator settings: (a) 0%, (b) 1%, (c) 2%, (d) 3%, and (e) 4% of the maximum voltage.

5. CONCLUSION

In this work, a circuit model of a commercial PCI generator is built based on frequency- and time-domain measurements at the external ports and suitable circuit parameter optimization. The proposed model is validated by measurement in an *ad-hoc* PCI test bench. The proposed model can be readily imported into general circuit solvers and used to improve the design and effectiveness of injection devices used for PCI testing.

6. REFERENCES

1. *Environmental Conditions and Test Procedures for Airborne Equipment, Section 20: Radio Frequency Susceptibility (Radiated and Conducted)*, RTCA DO-160F, Dec. 6, 2007.

2. *Electromagnetic Compatibility (EMC)—Part 4: Testing and Measurement Techniques—Section 6: Immunity to Conducted Disturbances, Induced by Radio Frequency Fields*, IEC 61000-4-6, Apr. 1996.

3. F. Grassi, G. Spadacini, F. Marliani, and S. A. Pignari, "Use of double bulk current injection for susceptibility testing of avionics," *IEEE Trans. Electromagn. Compat.*, vol. 50, no. 3, pp. 524–535, Aug. 2008.

4. L. Badini, G. Spadacini, F. Grassi, S. A. Pignari, P. Pelissou, "A rationale for statistical correlation of conducted and radiated susceptibility testing in aerospace EMC," *IEEE Trans. Electromagn. Compat.*, vol. 59, no. 5, pp. 1576-1585, Oct. 2017.

5. G. Spadacini, F. Grassi, S. A. Pignari, P. Bisognin and A. Piche, "Bulk Current Injection as an Alternative Radiated Susceptibility Test Enforcing a Statistically Quantified Overtesting Margin," *IEEE Trans. Electromagn. Compat.*, vol. 60, no. 5, pp. 1270-1278, Oct. 2018.

6. S. A. Pignari, G. Spadacini and F. Grassi, "Alternative radiated susceptibility test methods at unit level," *IEEE Electromagn. Compat. Mag.*, vol. 9, no. 1, pp. 61-68, 1st Quarter 2020.

7. *Space Engineering - EMC*, ECSS-E-ST-20–07C, Rev. 1, Feb. 2012.

8. *Requirements for the Control of Electromagnetic Interference Characteristics of Subsystems and Equipment, MIL-STD 461F*, Dec. 2007.

9. *Electromagnetic Compatibility (EMC) - Parts 2 - 10: Environment - Description of HEMP environment - Conducted disturbance*, IEC 61000- 2-10, 1998.

10. *High-altitude electromagnetic pulse (HEMP) protection for ground-based C41 facilities performing critical - Time-urgent missions - Part 1: Fixed facilities*, MIL-STD-188-125-1, 2005.

11. Z. Cui, F. Grassi, S. A. Pignari, B. Wei, "Pulsed current injection setup and procedure to reproduce intense transient electromagnetic disturbances," *IEEE Trans. Electromagn. Compat.*, vol. 60, no. 6, pp. 2065-2068, Dec. 2018.

12. Y. -H. Chen, Y. -Z. Xie, D. -Z. Zhang *et al.*, "10-kV transmission line experimental platform for HEMP immunity test of electrical equipment in operation," *IEEE Trans. Power Deliv.*, vol. 36, no. 2, pp. 1034-1040, April 2021.

13. montena technology sa., "PPG-E1-1200 datasheet: PCI - Short pulse portable generator." Accessed:

August 13, 2021. [Online]. Available: https://www.montena.com/fileadmin/technology_tests/documents/data_sheets/Data_sheet_PPG-E1-1200_generator.pdf.

14. Keysight Technologies, "PathWave Advanced Design System (ADS): Tuning and Optimization." Accessed: April 26, 2022. [Online]. Available: https://www.keysight.com/it/en/assets/7018-05133/technical-overviews/5992-1376.pdf.

15. X. Liu, F. Grassi, G. Spadacini *et al*., "Behavioral modeling of complex magnetic permeability with high-order Debye model and equivalent circuits," *IEEE Trans. Electromagn. Compat.*, vol. 63, no. 3, pp. 730-738, June 2021.

16. X. Liu, L. Crosta, F. Grassi *et al.*, "SPICE modeling of probes for pulse current injection," in *Proc. IEEE ESA Workshop Aerosp. EMC*, May 2019, pp. 1–6.